Acta Biochim Biophys Sin xxxx, xx(x): xx-xx
https://cstr.cn/32197.14.abbs.2026044
https://doi.org/10.3724/abbs.2026044
Original Article

Original Article

Ubiquitin-dependent degradation of MBD3 by TRIM59 promotes lung adenocarcinoma

Wenhui Yang[1,†], Jin Ren[2,†], Yufang Wang[1], Jiahe Shi[1], Ziwan Cai[1], Cuihong Cai[1], Jing Zheng[1], Jingjing Qu[1], and Jianya Zhou[1,*]

[1]Department of Respiratory Disease, Thoracic Disease Center, The First Affiliated Hospital, College of Medicine, Zhejiang University, Hangzhou 310003, China, and [2]State Key Laboratory of Molecular Biology, Shanghai Institute of Biochemistry and Cell Biology, Center for Excellence in Molecular Cell Science, Chinese Academy of Sciences, Shanghai 200031, China

[†]These authors contributed equally to this work.

*Correspondence address. E-mail: zhoujy@zju.edu.cn

Received 12 February 2026 Accepted 19 March 2026 Published 14 April 2026

Abstract

Methyl-CpG binding domain protein 3 (MBD3) functions as a critical tumor suppressor in lung adenocarcinoma (LUAD), yet the ubiquitin-dependent mechanisms orchestrating its proteasomal turnover remain elusive. Here, we demonstrate that MBD3 undergoes ubiquitination and identify tripartite motif-containing protein 59 (TRIM59) as the cognate E3 ligase. TRIM59 physically associates with the N-terminal MBD domain of MBD3 and catalyzes its polyubiquitination and degradation, and mass spectrometry mapping reveals that this process occurs primarily at lysine residues K41, K90, and K92. Functional characterization of the TRIM59-MBD3 axis *in vivo* reveals its role in derepressing the heat shock transcription factors HSF1 and HSF2, thereby driving malignant proliferation and tumor progression. Tissue microarray immunohistochemistry reveals that TRIM59 is upregulated, whereas MBD3 is downregulated in LUAD tissues, establishing an inverse expression pattern that supports oncogenesis. Our findings unveil an unappreciated layer of MBD3 regulation and identify the TRIM59-MBD3 ubiquitination cascade as a potential therapeutic vulnerability in LUAD.

Key words lung adenocarcinoma, MBD3, TRIM59, ubiquitination, HSF1/2

Introduction

Lung cancer remains the leading cause of cancer-related mortality worldwide, with lung adenocarcinoma (LUAD) representing the most common histological subtype [1]. Despite advances in targeted therapies and immunotherapy, the 5-year survival rate for advanced LUAD remains dismal, largely due to acquired drug resistance and metastatic progression [2,3]. This clinical challenge underscores the urgent need to elucidate the molecular mechanisms driving LUAD pathogenesis and to identify novel therapeutic targets that regulate tumor cell proliferation and survival.

Post-translational modifications, particularly ubiquitination, play pivotal roles in maintaining protein homeostasis and regulating cellular signaling pathways implicated in cancer development [4,5]. The ubiquitin-proteasome system (UPS) mediates the selective degradation of key regulatory proteins, with E3 ubiquitin ligases serving as critical determinants of substrate specificity [4]. Dysregulation of E3 ligase activity frequently contributes to oncogenesis, either through the destabilization of tumor suppressors or the stabilization of oncoproteins [6–9]. Understanding the specific E3 ligase-substrate networks operational in cancer cells therefore offers significant potential for therapeutic intervention.

Methyl-CpG binding domain protein 3 (MBD3) is an essential core component of the nucleosome remodeling and deacetylase (NuRD) complex, which dynamically regulates gene expression through ATP-dependent chromatin remodeling and histone deacetylation [10]. Functioning as a versatile DNA-binding protein, MBD3 preferentially recognizes unmethylated CpG islands within gene promoters, recruiting the NuRD complex to modulate local chromatin architecture and accessibility [10,11]. While traditionally recognized for its role in transcriptional repression through histone deacetylation and chromatin compaction, accumulating evidence indicates that MBD3 can also facilitate transcriptional activation depending on the cellular context, specific genomic loci, and interacting cofactors [12,13]. This dual role, as both a transcrip-

© The Author(s) 2026. This is an open access article distributed under the terms of the Creative Commons Attribution-NonCommercial-NoDerivs License (https://creativecommons.org/licenses/by-nc-nd/4.0/).

tional repressor and activator, allows MBD3 to precisely coordinate complex gene expression programs critical for cell differentiation, development, and tissue homeostasis.

In this study, we demonstrate that MBD3 is significantly downregulated in LUAD, functioning as a tumor suppressor by suppressing cancer cell proliferation and clonogenic growth. While MKRN3 has been previously reported to ubiquitinate MBD3, this modification does not trigger proteasomal degradation [12], leaving the mechanism underlying MBD3 destabilization unclear. Here, we identified TRIM59 as the bona fide E3 ubiquitin ligase responsible for MBD3 degradation in lung adenocarcinoma cells and systematically elucidated the functional significance of this TRIM59-MBD3 signaling axis in LUAD progression.

Materials and Methods

Data analysis using public databases

To compare MBD3 expression between tumor and normal tissues, we analyzed RNA sequencing data from two public databases. Tumor samples were obtained from The Cancer Genome Atlas (TCGA) via the UCSC Xena platform (https://xena.ucsc.edu/), while normal tissue controls were retrieved from the Genotype-Tissue Expression (GTEx) project. *MBD3* mRNA levels were extracted and normalized across samples. Differential expression between tumor and normal groups was assessed using the Wilcoxon rank-sum test.

GEPIA2 (http://gepia2.cancer-pku.cn), an online platform for gene expression analysis based on data from TCGA and the Genotype-Tissue Expression (GTEx) projects [14], was utilized in this study to investigate the mRNA expression patterns of *MBD3* and *TRIM59* in LUAD. Differential expression between tumor and normal tissues was evaluated using Student's *t* test, with statistical significance defined as an absolute log2(fold change) ≥ 0.5 and $P < 0.05$. Furthermore, the prognostic implications of MBD3 and TRIM59 expressions were assessed by analyzing their association with overall survival in LUAD patients.

Cell culture, transfection and reagents

Human lung adenocarcinoma cell lines A549, H1975 and HEK293T cells were obtained from the Cell Bank of the Chinese Academy of Sciences (Shanghai, China) and maintained in RPMI-1640 medium (Witcel, Shanghai, China) supplemented with 10% fetal bovine serum (FBS; Gibco, Carlsbad, USA), 100 U/mL penicillin, and 100 μg/mL streptomycin (Beyotime, Shanghai, China). Cultures were incubated at 37°C in a humidified atmosphere containing 5% CO_2. For plasmid transfection, cells were treated with T103 LipoMAX 3000 transfection reagent (Witcel) according to the manufacturer's instructions. Stable transfectants were established by continuous selection with 2 μg/mL puromycin (Beyotime) for a minimum of seven days. Cycloheximide (CHX; Selleck, Houston, USA) was dissolved in dimethyl sulfoxide (Sigma-Aldrich, St Louis, USA) at a concentration of 100 mM and stored at −80°C. A549 and H1975 cells were treated with 100 μM CHX for 6 h or different time periods at 37°C. For protein degradation pathway analysis, A549 cells were treated with 1 μM proteasomal inhibitor bortezomib (BTZ; Selleck) or 20 nM autophagy inhibitor bafilomycin (BAF; Selleck) for 6 h at 37°C prior to western blot analysis.

Plasmid construction

Full-length and truncated cDNA sequences encoding *MBD3* and *TRIM59* were amplified from HEK293T cells and subsequently cloned and inserted into the following expression vectors all purchased from Miaolingbio (Wuhan, China): pCDH (lentiviral expression), pcDNA3.0-Flag/MYC (mammalian expression with epitope tags), pET22b (bacterial expression), and pGEX-4T-1 (glutathione S-transferase fusion, bacterial expression). TRIM59 and MBD3 site-directed mutagenesis was performed to introduce point mutations as previously described [15]. For CRISPR-mediated gene knockout, single-guide RNAs (sgRNAs) targeting *MBD3* and *TRIM59* were designed and synthesized as oligonucleotides (YOCON Biotechnology, Beijing, China). Following annealing, the sgRNA oligos were ligated into the *Bsm*BI-digested lentiCRISPR v2 vector (Thermo Fisher Scientific, Waltham, USA) using T4 DNA ligase (NEB, Ipswich , USA). The sgRNA sequences are provided in Supplementary Table S1.

Generation of knockout cell lines

CRISPR-Cas9-mediated knockout (KO) of *MBD3* and *TRIM59* was performed as previously described [12]. Briefly, A549 and H1975 cells were transduced with lentiCRISPR v2 lentivirus (Miaolingbio) encoding gene-specific sgRNAs and subjected to selection with 2 μg/mL puromycin for 2 weeks. Successful knockout was confirmed by immunoblot analysis demonstrating complete loss of target protein expression.

CCK-8 assay

A549 and H1975 cells (wild-type, overexpression or knockout) were seeded into 96-well plates at a density of 5000 cells per well and allowed to attach for 6 h. Cell proliferation was then monitored at designated time points (0, 24, 48, and 72 h), where the 0 h reading served as the baseline. At each time point, 10 μL of CCK-8 reagent (Beyotime) was added to each well, followed by incubation at 37°C for 3 h. Absorbance was measured at 450 nm using a microplate reader (Bio-Rad Laboratories, Hercules, USA). All experiments were performed in six replicates.

Colony formation assay

A549 and H1975 cells (wild-type, overexpression or knockout) were seeded into 6-well plates at a density of 1000 cells per well. Following incubation at 37°C for 7 days with medium changes every 2–3 days, cells were fixed with 4% paraformaldehyde (Beyotime) for 10 min at room temperature and subsequently stained with 0.2% crystal violet (Beyotime) for 15 min. Colony formation was documented using an iPhone 14 camera (Apple Inc., Cupertino, USA), and colonies containing ≥ 50 cells were manually enumerated under an inverted microscope (CKX53; Olympus, Tokyo, Japan).

Identification of MBD3-interacting proteins by mass spectrometry

A549 cells seeded in six 10-cm dishes were transfected with either empty vector or pcDNA3.0-MBD3-Flag using T103 LipoMAX 3000 and cultured for 48 h. Cells were then lysed in Co-IP buffer (50 mM Tris-HCl, 150 mM NaCl, 5 mM EDTA, and 1% NP-40, pH 7.6) supplemented with protease inhibitor cocktail (Selleck) and incubated with anti-Flag affinity gel (Biolinkedin, Shanghai, China) at 4°C overnight. Immunoprecipitates were washed three times with Co-IP buffer and eluted with 8 M urea in 100 mM Tris-HCl (pH 8.0). Eluted proteins were subjected to reduction with TCEP (Millipore, Billerica, USA), alkylation with chloroacetamide (CAA)

(Millipore), and digestion with trypsin, followed by mass spectrometry analysis. Raw MS data were processed as previously described [16]. Differentially expressed proteins (DEPs) were defined as those detected (intensity > 0) in at least three samples. Missing values were imputed using the minimum intensity value across the proteome dataset, followed by quantile normalization. Differential expression analysis was performed using one-sided Student's *t* tests implemented in R software (https://www.r-project.org), with *P* values adjusted by the Benjamini-Hochberg method. Proteins with an adjusted *P* value ≤ 0.05 and $\log_2$fold change ≥ 2 were considered significantly upregulated. An adjusted *P* value < 0.05 was considered statistically significant.

Co-immunoprecipitation, immunoprecipitation and immunoblotting

For co-immunoprecipitation (Co-IP) assays, A549 or H1975 cells were lysed in 1 mL of Co-IP buffer (50 mM Tris-HCl, 150 mM NaCl, 5 mM EDTA, and 1% NP-40, pH 7.6) supplemented with a protease-inhibitor cocktail (Selleck). After centrifugation, the supernatant was incubated overnight at 4°C with an anti-MBD3 antibody (1:50 dilution; 14258-1-AP; Proteintech, Wuhan, China) or control rabbit IgG (1:50 dilution; 30000-0-AP; Proteintech) and Protein G magnetic beads (L-1002; Biolinkedin). For immunoprecipitation (IP) assays, cells transfected with the indicated plasmids were lysed in 1 mL RIPA buffer (150 mM NaCl, 50 mM Tris-HCl, 5 mM EDTA, 1% NP-40, and 0.1% SDS, pH 7.6) freshly supplemented with protease inhibitor cocktail. The lysates were incubated overnight at 4°C with anti-Flag affinity gels (Biolinkedin). The next day, the immunoprecipitates were washed three times with Co-IP/IP buffer and denatured at 100°C for 10 min in 50 μL of 2× SDS loading buffer. Immunoprecipitates and input samples were resolved on 10% SDS-PAGE gels and transferred to PVDF membranes (Millipore). Membranes were blocked with 10% (w/v) skim milk for 1 h at room temperature and then incubated overnight at 4°C with the following primary antibodies (all from Proteintech): anti-MBD3 (1:1000; 14258-1-AP), anti-TRIM59 (1:1000; 28575-1-AP), anti-GAPDH (1:5000; 60004-1-Ig), anti-GST-HRP (1:10,000; HRP-66001), anti-His-HRP (1:1000; HRP-66005), anti-Flag (1:2000; 80010-1-RR), anti-HA (1:1000; 51064-2-AP), anti-HSF1 (1:500; 51034-1-AP) or anti-HSF2 (1:1000; 10706-1-AP). After washing three times with TBST (50 mM Tris-HCl, 150 mM NaCl and 0.2% Tween-20, pH 8.0), membranes were incubated with HRP-conjugated secondary antibodies (goat anti-rabbit IgG: 1:5000; SA00001-2 and goat anti-mouse IgG: 1:5000; SA00001-1; Proteintech) for 1 h at room temperature. Protein bands were visualized using enhanced chemiluminescence (ECL) reagent (Tanon, Beijing, China) and detected with a Tanon 5200 imaging system (Tanon).

Recombinant protein purification

GST- and His6-tagged fusion proteins were expressed in *Escherichia coli* BL21(DE3). Protein expression was induced by adding 1 mM isopropyl β-*D*-1-thiogalactopyranoside (IPTG; Sangon Biotech, Shanghai, China) and incubating for 16 h at 37°C. Bacterial cells were harvested by centrifugation, resuspended in PBS (pH 8.0) containing 1 mM PMSF (Beyotime), and lysed by sonication on ice. Clarified lysates were incubated with glutathione-Sepharose 4B or Ni-NTA agarose (Biolinkedin) for 4 h at 4°C. The beads were subsequently washed three times with PBS (pH 8.0) containing 0.1% Triton X-100. Bound proteins were eluted with 20 mM reduced L-glutathione (pH 8.0) for GST-tagged proteins or 500 mM imidazole (pH 8.0) for His6-tagged proteins. Eluates were dialyzed overnight at 4°C against PBS (pH 8.0) containing 20% glycerol and subsequently stored at −80°C.

GST pull-down assay

Purified His6-tagged and GST-tagged proteins (10 μg each) were combined and incubated overnight at 4°C with 50 μL glutathione-agarose beads (Biolinkedin) in 1 mL ice-cold GST pull-down buffer (20 mM Tris-HCl pH 8.0, 100 mM NaCl, 5 mM $MgCl_2$, 1 mM EDTA, 0.5% NP-40, 1 mM DTT, and 10 mg/mL fresh BSA) with gentle rotation. The beads were collected by brief centrifugation and washed three times with 1 mL of the same buffer. Bound proteins were eluted by boiling in 2× SDS loading buffer for 10 min and analyzed by 10% SDS-PAGE followed by immunoblotting.

Structure prediction of the TRIM59-MBD3 complex

Structural modeling of the TRIM59-MBD3 complex was performed using AlphaFold Server (https://alphafoldserver.com/) as previously described [16]. The top-ranked model, selected based on the highest AlphaFold 3 confidence score (ipTM + pTM), was used for subsequent analysis. Protein-protein interaction interfaces were visualized and analyzed using PyMOL (https://pymol.org/PyMOL), with interfacial residues defined as those positioned within 5 Å of the binding partner. Key residues potentially mediating non-covalent interactions, including hydrogen bonds, salt bridges, and π-π stacking, were subsequently identified based on structural geometry and annotated by residue number.

In vitro ubiquitination assay

In vitro ubiquitination was performed as described previously [17]. Briefly, reaction mixtures (50 μL final volume) containing recombinant His6-UBA1 (100 ng; E1 ubiquitin-activating enzyme), His6-UBCH5A (100 ng; E2 ubiquitin-conjugating enzyme), GST-TRIM59 (100 ng; E3 ubiquitin ligase), MBD3-His6 (200 ng), and His6-ubiquitin (100 ng) were prepared in ubiquitination buffer (25 mM Tris-HCl, pH 7.8, 100 mM NaCl, 5 mM $MgCl_2$, 1 mM ATP, and 0.5 mM DTT) and incubated at 37°C for 1 h. Subsequently, His6-Usp2cc (50 ng) was added to the reaction mixture and incubated at 37°C for an additional 30 min. Ubiquitination of MBD3 was analyzed by immunoblotting using anti-MBD3 antibody.

Mapping of MBD3 ubiquitination sites

Ubiquitinated MBD3 recovered from the *in vitro* ubiquitination assay was subjected to ubiquitin-site mapping as previously described [6]. Briefly, the protein was dissolved in 8 M urea/100 mM Tris-HCl (pH 8.0), reduced with TCEP, alkylated with NEM, and digested with trypsin. The resulting peptides were separated using an EASY-nLC system (Thermo Fisher Scientific) and analyzed on a Q Exactive mass spectrometer (Thermo Fisher Scientific). Data were processed with Proteome Discoverer 2.1 (Thermo Fisher Scientific) against the UniProt human database (www.uniprot.org).

Database mining for MBD3-binding targets

To identify *MBD3* downstream targets, we performed an integrative analysis of DNA-binding data from two independent databases. First, MBD3-binding sequences were retrieved from the HTP-SELEX database (http://floresta.eead.csic.es/htpselex), which provides

high-throughput *in vitro* DNA-binding specificities for transcription factors. These data were then cross-referenced with *MBD3* target gene annotations from the TRANSFAC database (https://genexplain.com/transfac/), a curated repository of eukaryotic transcription factors and their binding sites. Overlapping targets common to both databases were selected to ensure high confidence. This integrative approach yielded 10 candidate target genes for subsequent functional validation.

Chromatin immunoprecipitation assay

Chromatin immunoprecipitation (ChIP) was performed using the ChIP Assay kit (Beyotime) according to the manufacturer's protocol. Briefly, A549 cells were cross-linked with 1% formaldehyde (Beyotime) for 10 min at room temperature, followed by quenching with 125 mM glycine for 5 min. Cells were washed twice with ice-cold PBS and resuspended in 270 μL lysis buffer (50 mM Tris-HCl, pH 8.0, 10 mM EDTA, 1% SDS, and protease inhibitor cocktail) for 5 min on ice. Chromatin was sheared using a Bioruptor UCD-300 (Diagenode, Liège, Belgium) for 30 cycles (30 s on, 30 s off) at high power setting. Lysates were centrifuged at 13,000 *g* for 10 min at 4°C, and 100 μL of the supernatant was diluted 10-fold with ChIP dilution buffer (20 mM Tris-HCl, pH 8.0, 0.01% SDS, 1.1% Triton X-100, 1.1 mM EDTA, and 167 mM NaCl) and then incubated overnight at 4°C with 5 μg of control rabbit IgG or anti-MBD3 antibody.

The following day, the samples were incubated with 40 μL of Protein G magnetic beads for 2 h at 4°C. The beads were subsequently washed sequentially: three times with low-salt wash buffer (20 mM Tris-HCl, pH 8.0, 150 mM NaCl, 0.1% SDS, 1% Triton X-100, and 2 mM EDTA), three times with high-salt wash buffer (20 mM Tris-HCl, pH 8.0, 500 mM NaCl, 1% NP-40, 0.1% SDS, and 2 mM EDTA), three times with LiCl wash buffer (20 mM Tris-HCl, pH 8.0, 500 mM LiCl, 1% NP-40, 1% deoxycholate, and 1 mM EDTA), and three times with TE buffer (10 mM Tris-HCl, pH 8.0, and 1 mM EDTA). Washed beads were resuspended in 200 μL elution buffer (1% SDS and 0.1 M $NaHCO_3$) and incubated at 65°C for 30 min with agitation. Eluted chromatin was reverse cross-linked at 65°C for 4 h after adjusting NaCl to a final concentration of 300 mM, followed by proteinase K digestion (50 μg) at 55°C for 1 h. DNA was purified using the phenol-chloroform extraction method and analyzed by ChIP-qPCR. The sequences of primers used in this study are listed in Supplementary Table S2.

Reverse transcription PCR and quantitative real-time PCR

Total RNA was extracted using the RNAsimple Total RNA kit (Tiangen, Beijing, China) according to the manufacturer's protocol. cDNA was synthesized using ReverTra Ace qPCR RT Master Mix (Toyobo, Tokyo, Japan). Quantitative real-time PCR (qPCR) was performed using SYBR Green Master Mix (Toyobo) on a 7500 Real-Time PCR System (Applied Biosystems, Foster City, USA), QuantStudio 6 Flex Real-Time PCR System (Thermo Fisher Scientific), or LightCycler 96 System (Roche, Basel, Switzerland). Relative gene expression levels were normalized to *GAPDH* and calculated using the $2^{-\Delta\Delta Ct}$ method. The sequences of primers used in this study are listed in Supplementary Table S3.

Tumor xenograft assay

Four-week-old male athymic nude mice were purchased from Shanghai SLAC Laboratory Animal Co., Ltd (Shanghai, China) and acclimatized for one week prior to tumor cell inoculation. All animal procedures were approved by the Institutional Animal Care and Use Committee of the First Affiliated Hospital, Zhejiang University School of Medicine (No. 2026-066) and performed in accordance with institutional guidelines. A549 cells (1×10^7 cells per mouse) of the indicated genotypes were subcutaneously injected into the right flank (six mice per group). Due to the relatively slow growth rate of this cell line, tumor dimensions were measured every 6 days using a digital caliper, and volumes were calculated using the formula: $V = 0.5 \times (\text{length} \times \text{width}^2)$. On day 30, the mice were sacrificed; the tumors were excised, weighed, and lysed in RIPA buffer for immunoblot analysis.

Immunohistochemistry

Human LUAD tissue microarrays (TMAs) were purchased from Shanghai CellResearcher Biotechnology Co., Ltd (Shanghai, China). Immunohistochemistry was performed as previously described [18] with minor modifications. Briefly, TMA sections were deparaffinized in xylene and rehydrated through a graded ethanol series. Antigen retrieval was conducted by microwave heating in 0.01 M sodium citrate buffer (pH 6.0) for 30 min. Endogenous peroxidase activity was quenched with 3% hydrogen peroxide, followed by blocking with 10% normal goat serum for 30 min at room temperature. Sections were then incubated overnight at 4°C with primary antibodies against MBD3 (1:200; 14258-1-AP) or TRIM59 (1:200; 28575-1-AP) (both from Proteintech). Detection was performed using the Universal IHC Staining Kit (PK10006; Proteintech) according to the manufacturer's protocol.

Whole-slide images were acquired using a 3DHISTECH DX150 slide scanner (3DHISTECH, Budapest, Hungary) at 20× magnification (0.5 μm/pixel resolution). Immunohistochemical staining was evaluated by two independent pathologists who were blinded to the clinical data. Staining intensity was scored on a scale of 0–3 (0, negative; 1, weak; 2, moderate; and 3, strong), and the percentage of positive tumor cells was categorized as 0 (0%–5%), 1 (6%–25%), 2 (26%–50%), 3 (51%–75%), or 4 (> 75%). The immunoreactivity score (IRS) was calculated by multiplying the intensity score by the percentage score, yielding values ranging from 0 to 12. Statistical analyses were performed using GraphPad Prism 10 (GraphPad Software, San Diego, USA).

Statistical analysis

Data are presented as the mean ± standard deviation (SD) and analyzed using GraphPad Prism 10. Comparisons between two groups were performed using two-tailed unpaired Student's *t* tests, whereas multiple group comparisons were conducted using one-way ANOVA followed by Tukey's *post hoc* test. Statistical significance was defined as $P < 0.05$.

Results

MBD3 inhibits the proliferation of lung adenocarcinoma cells

Pan-cancer analysis of *MBD3* mRNA expression comparing TCGA tumors with GTEx normal controls revealed that MBD3 is significantly downregulated in LUAD (Figure 1A). Although the correlation between *MBD3* expression and overall survival failed to achieve statistical significance, LUAD patients with elevated *MBD3* expression exhibited a favorable survival trend (Supplementary

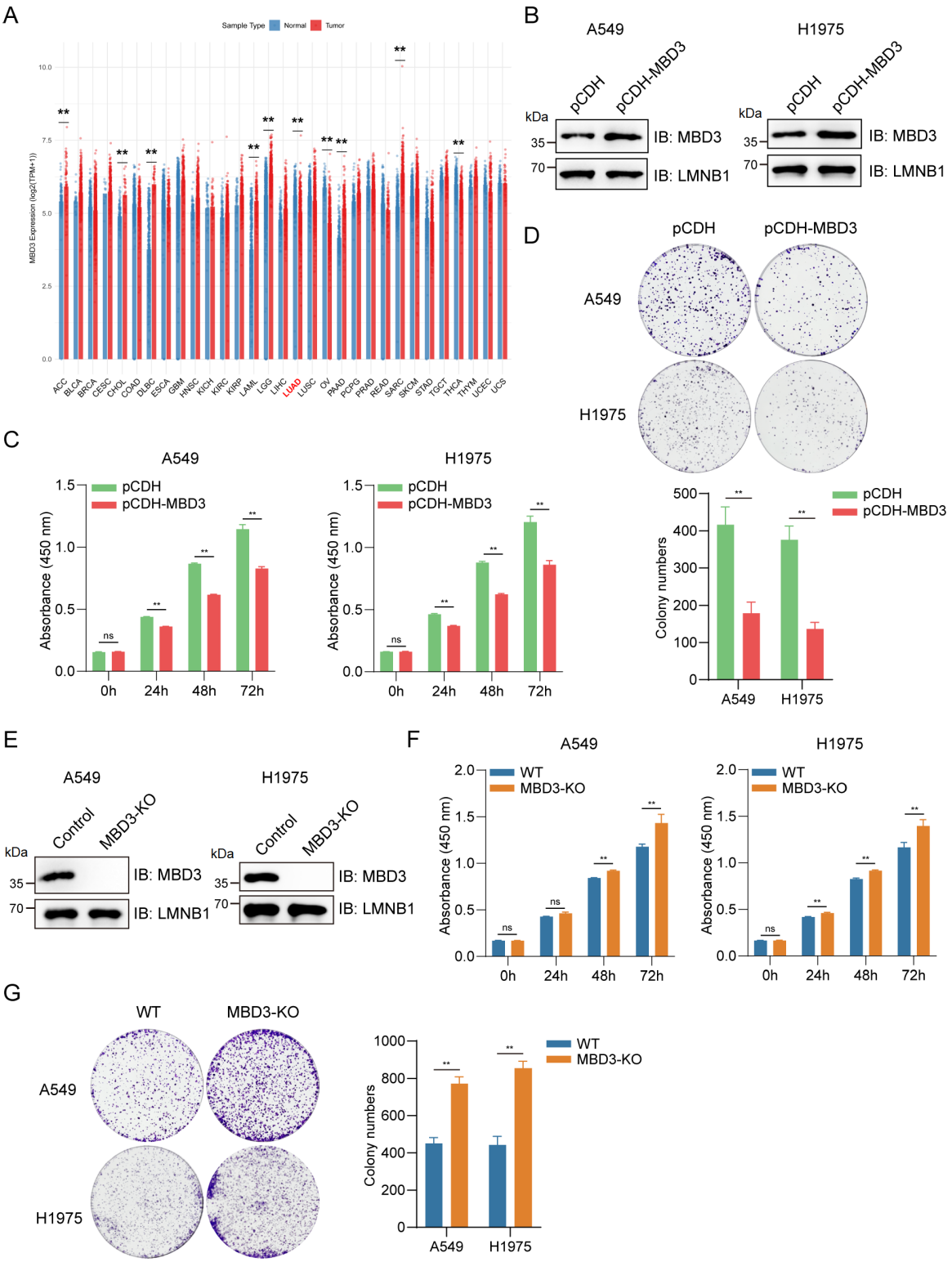


Figure 1. MBD3 inhibits the proliferation of lung adenocarcinoma cells (A) *MBD3* mRNA levels in TCGA tumors versus GTEx normal controls. Data sourced from UCSC Xena. *P* values were calculated using the Wilcoxon rank-sum test. (B) Verification of MBD3 overexpression in A549 and H1975 cells by immunoblotting. (C) CCK-8 assays revealed that MBD3 overexpression inhibits the proliferation of A549 and H1975 cells. Six replicates per group were performed. (D) Colony formation assays showed that MBD3 overexpression suppresses the clonogenic capacity of A549 and H1975 cells. Three replicates per group were performed. (E) Establishment of *MBD3*-knockout A549 and H1975 cell lines verified by immunoblotting. (F) CCK-8 assays revealed that *MBD3* knockout promotes the proliferation of A549 and H1975 cells. Six replicates per group were performed. (G) Colony formation assays showed that *MBD3* knockout enhances the clonogenic capacity of A549 and H1975 cells. Three replicates per group were performed. $^{**}P < 0.01$. ns, no significant difference.

Figure S1). Stable *MBD3*-overexpressing cell lines were generated in A549 and H1975 cells, with overexpression efficiency validated by immunoblotting (Figure 1B). CCK-8 and colony formation assays revealed that *MBD3* overexpression significantly inhibited the proliferation of both A549 and H1975 lung adenocarcinoma cells (Figure 1C,D). Conversely, *MBD3*-knockout A549 and H1975 cell lines exhibited enhanced proliferative capacity compared to controls (Figure 1E–G).

TRIM59 interacts with MBD3

Given the significant impact of MBD3 on lung adenocarcinoma cells, the protein degradation pathways were subsequently investigated. A549 cells were treated with the proteasomal inhibitor BTZ or the autophagy inhibitor BAF for 6 h prior to immunoblot analysis, revealing that MBD3 is primarily degraded via the proteasome (Figure 2A).

To identify the E3 ubiquitin ligase responsible for MBD3 degradation, Flag-tagged MBD3 was transfected into A549 cells and used as bait for Co-IP to capture interacting proteins. MS analysis identified MKRN3 and TRIM59 as the highest-confidence E3 ligase candidates (Figure 2B). Although MKRN3 has been previously reported as an E3 ligase for MBD3, it did not mediate MBD3 degradation under these experimental conditions [12]; therefore, TRIM59 was selected for further investigation.

The interaction between TRIM59 and MBD3 was subsequently validated. Endogenous Co-IP demonstrated that MBD3 forms a complex with TRIM59 (Figure 2C), while a GST pull-down assay confirmed their direct physical interaction (Figure 2D). Domain mapping demonstrated that the N-terminal RING domain of TRIM59 directly binds to the N-terminal MBD domain of MBD3 (Figure 2E,F), consistent with the AlphaFold3-predicted complex structure (Figure 2G).

TRIM59 ubiquitinates MBD3

To determine whether TRIM59 ubiquitinates MBD3, *in vivo* and *in vitro* ubiquitination assays were performed. Exogenous MBD3 was efficiently ubiquitinated by wild-type TRIM59 but not by the E3 ligase-dead C30/33A mutant (Figure 3A). *In vitro* reactions containing purified E1 (UBA1), E2 (UBCH5A), and E3 (TRIM59) confirmed MBD3 ubiquitination, which was abolished by the catalytic core of the human deubiquitinase USP2 (Usp2cc) (Figure 3B). MS analysis of MBD3 recovered from the *in vitro* ubiquitination assay (Figure 3C) identified ubiquitination at eight lysine residues. Among these, K41, K90, and K92 were validated as the major sites for TRIM59-mediated ubiquitination in A549 cells (Figure 3D,E).

TRIM59 mediates the degradation of MBD3

In A549 cells, the TRIM59-dependent reduction in MBD3 protein levels was almost completely blocked by the proteasome inhibitor BTZ but remained unaffected by the autophagy inhibitor BAF (Figure 4A). Furthermore, TRIM59 reduced MBD3 protein levels in a dose-dependent manner in both A549 and H1975 cells (Figure 4B).

CRISPR/Cas9-mediated *TRIM59*-KO cells were established (Figure 4C). Loss of *TRIM59* stabilized MBD3 protein levels, whereas reintroduction of wild-type TRIM59 restored rapid MBD3 turnover in both A549 and H1975 cells (Figure 4D). Notably, the ubiquitination-deficient *MBD3* mutant (K41/90/92R) resisted TRIM59-mediated degradation (Figure 4E), confirming that site-specific ubiquitination is required for MBD3 instability.

TRIM59 regulates HSF1/2 signaling via MBD3-mediated transcriptional control

The mRNA expression of *TRIM59* in human LUAD was analyzed using the GEPIA2 database. As shown in Figure 5A, *TRIM59* expression was significantly upregulated in LUAD tissues compared with adjacent normal controls. Furthermore, the association between *TRIM59* expression and clinical outcomes was evaluated, revealing that LUAD patients with low *TRIM59* mRNA levels exhibited significantly improved overall survival (Figure 5B).

To explore the functional significance of TRIM59-mediated MBD3 ubiquitination, *TRIM59*/*MBD3* double-knockout cell lines were established in A549 and H1975 cells and validated by immunoblotting (Figure 5C). Colony formation assays revealed that *TRIM59* depletion significantly inhibited the clonogenic capacity of both cell lines. Notably, this inhibitory effect was completely abrogated in *TRIM59*/*MBD3* double-knockout cells compared to *MBD3* knockout alone, indicating that the suppressive effect of *TRIM59* depletion on cell proliferation is mediated through MBD3 (Figure 5D).

MBD3 is a DNA-binding protein that preferentially binds to unmethylated DNA. By integrating *MBD3* target gene annotations from the HTPSELEX and TRANSFAC databases, 10 high-confidence targets were identified (Figure 5E). Among these, *HSF1*, *HSF2*, *FOXD3*, *HOXA13*, *FOXL1* and *HOXD8* were selected for further validation based on their established relevance to lung cancer. ChIP assays in A549 cells demonstrated that MBD3 binds to the promoters of *HSF1*, *HSF2*, *HOXA13*, *FOXL1* and *HOXD8* (Figure 5F). However, qPCR analysis revealed that *MBD3* knockout selectively affected the expressions of only *HSF1/2* (Figure 5G). Importantly, *TRIM59* knockout suppressed *HSF1/2* expressions via an MBD3-dependent mechanism, as concurrent knockout of *MBD3* rescued HSF1/2 levels in both A549 and H1975 cells (Figure 5H).

TRIM59 knockout suppresses LUAD growth via MBD3-dependent HSF1/2 signaling

A xenograft tumorigenicity model in nude mice was employed to investigate the functional role of TRIM59-MBD3 signaling in LUAD. *TRIM59* knockout markedly suppressed tumor growth; however, this inhibitory effect was completely abolished upon concurrent *MBD3* knockout (Figure 6A). At 30 days post-injection, tumors from the *TRIM59* knockout group exhibited significantly reduced weight compared to controls, whereas additional *MBD3* knockout reversed the effect of *TRIM59* ablation on tumor burden. Notably, *MBD3* knockout alone resulted in significantly increased tumor weight compared to MBD3-intact controls (Figure 6B,C). Immunoblotting of excised tumors confirmed that *TRIM59* knockout-mediated tumor suppression coincided with MBD3 stabilization and consequent destabilization of HSF1 and HSF2. These effects were dependent on MBD3, as concurrent *MBD3* knockout reversed the phenotype (Figure 6D).

Finally, clinical validation using LUAD tissue microarrays showed that TRIM59 was upregulated in cancer tissues compared to adjacent normal tissues (Figure 6E), while MBD3 was conversely downregulated in tumors (Figure 6F).

Collectively, these findings support a working model wherein TRIM59-mediated ubiquitination targets MBD3 for proteasomal degradation, consequently derepressing HSF1/2 transcriptional activity to facilitate LUAD progression (Figure 6G).

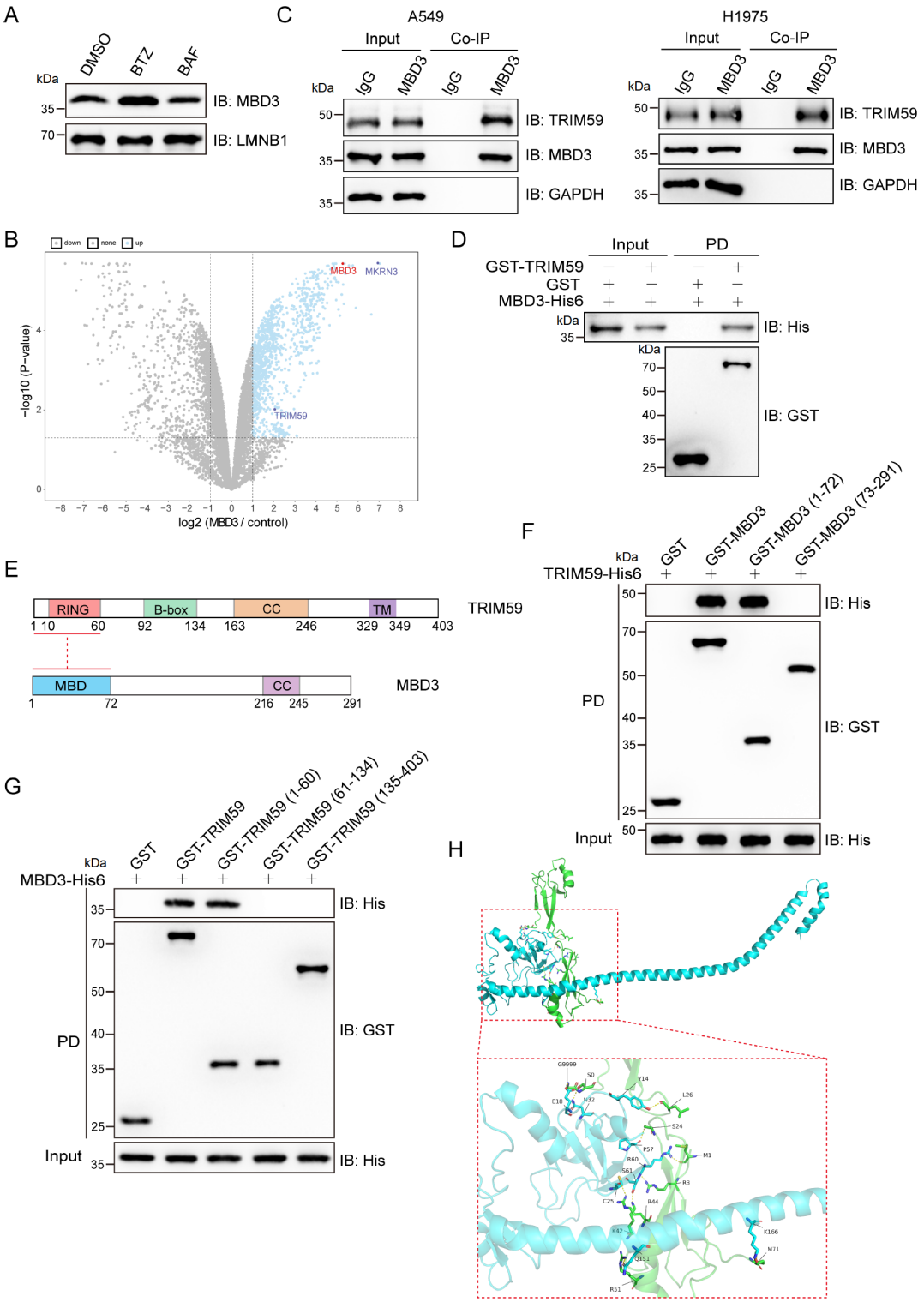


Figure 2. TRIM59 interacts with MBD3 (A) Immunoblot analysis revealed that MBD3 is primarily degraded via the proteasome. A549 cells were treated for 6 h with bortezomib (BTZ, 1 μM), bafilomycin A1 (BAF, 20 nM), or cycloheximide (CHX, 100 μg/mL) before harvest. (B) Identification of MBD3-interacting proteins by coimmunoprecipitation coupled with mass spectrometry (Co-IP/MS). Volcano plots depict differentially enriched proteins between MBD3 and control immunoprecipitates ($n = 3$ per group). (C) Endogenous MBD3 interacts with TRIM59 in A549 and H1975 cells. Cell lysates were subjected to immunoprecipitation using an anti-MBD3 antibody, followed by immunoblotting with the indicated antibodies. (D) Direct interaction between TRIM59 and MBD3. A GST pull-down assay was performed using recombinant GST-TRIM59 and His6-MBD3 proteins. (E-G) The RING domain of TRIM59 interacts with the MBD domain of MBD3. GST pull-down assays were performed using purified recombinant GST-TRIM59 and His6-MBD3 domain constructs as indicated. (H) Structural model of the TRIM59-MBD3 interaction predicted by AlphaFold 3 and rendered in PyMOL.

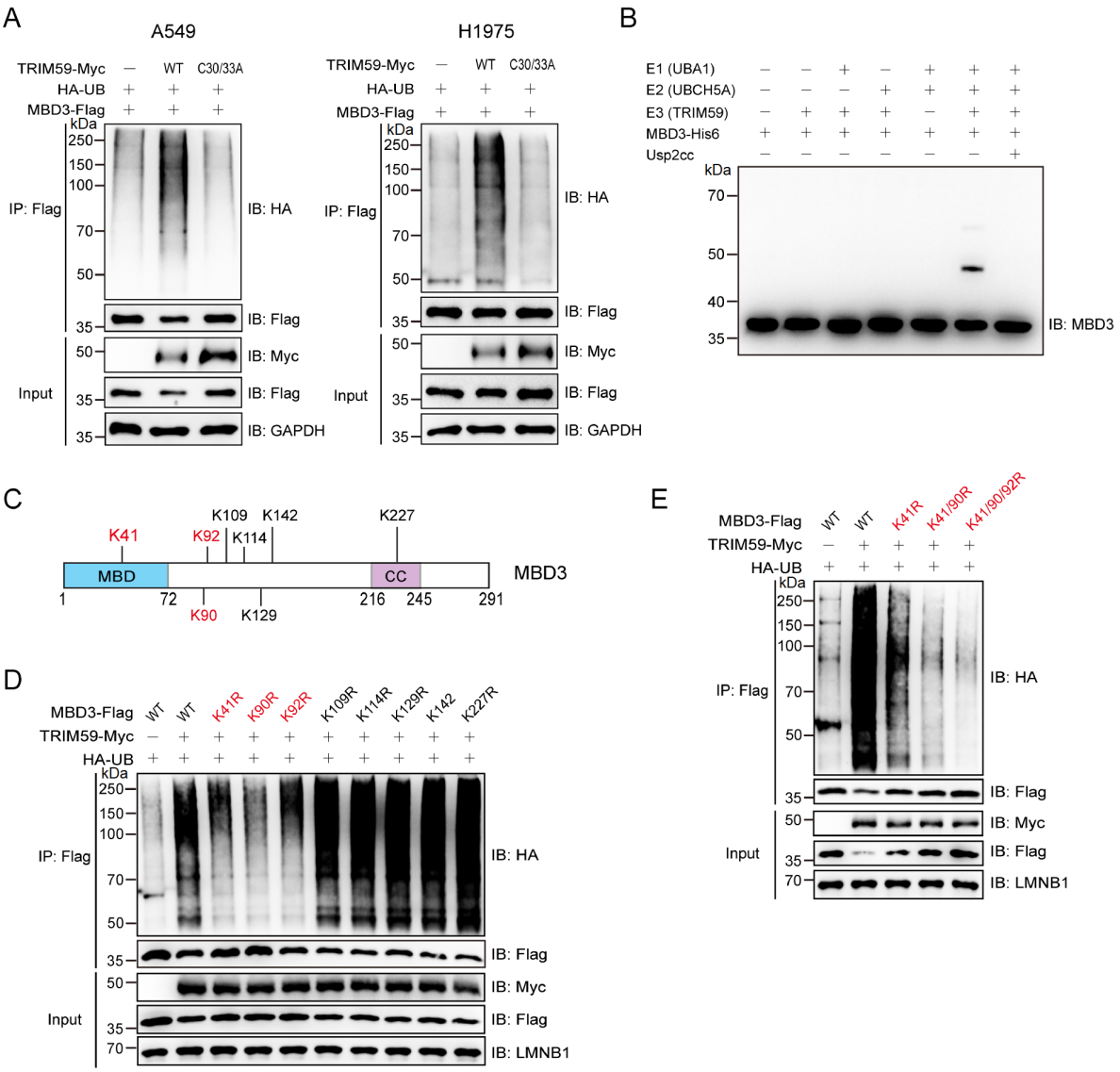


Figure 3. TRIM59 ubiquitinates MBD3 (A) TRIM59-Myc mediates ubiquitination of Flag-MBD3. A549 and H1975 cells were co-transfected with the indicated plasmids; lysates were subjected to immunoprecipitation with anti-Flag affinity gel followed by immunoblotting. TRIM59-C30/33A denotes an E3 ligase-dead mutant. (B) TRIM59 ubiquitinates MBD3 *in vitro*. An *in vitro* ubiquitination assay was performed using recombinant MBD3-His6, His6-UBA1 (E1), UBCH5A (E2), GST-TRIM59 (E3), or His6-Usp2cc (catalytic core of human deubiquitinase USP2) as indicated, followed by immunoblotting. (C) Schematic representation of eight TRIM59-mediated ubiquitination sites on MBD3. Ubiquitinated MBD3 was recovered from the *in vitro* ubiquitination assay (panel B) and analyzed by MS to identify the specific sites. (D,E) TRIM59-mediated ubiquitination of MBD3 occurs primarily at three major sites: K41, K90, and K92. A549 cell lysates ectopically expressing the indicated Flag-tagged MBD3 mutants were immunoprecipitated with anti-Flag affinity beads and analyzed by immunoblotting.

Discussion

Through comprehensive functional analyses, this study demonstrates that MBD3 functions as a tumor suppressor in LUAD and is significantly downregulated in tumor tissues compared with normal controls (Figures 1A,6F). Mechanistic investigations identified TRIM59 as a novel E3 ubiquitin ligase responsible for MBD3 degradation, which directly binds to the N-terminal MBD domain of MBD3 via its RING domain and catalyzes polyubiquitination at lysine residues K41, K90, and K92 (Figures 2–4). This posttranslational modification leads to derepression of *HSF1* and *HSF2* transcription, consequently promoting malignant proliferation and clonogenic growth in both *in vitro* assays and xenograft models (Figures 5,6). These findings establish a novel post-translational regulatory network linking the ubiquitin-proteasome system to the epigenetic control of heat shock transcription factors.

Previous studies identified MKRN3 as an E3 ligase that ubiquitinates MBD3 without triggering proteasomal degradation, instead regulating protein-protein interactions [12]. In contrast, TRIM59 catalyzes degradative ubiquitination of MBD3. The mapping of specific ubiquitination sites (K41, K90, and K92) and the resistance of the K41/90/92R mutant to TRIM59-mediated degradation confirm this as a distinct regulatory mechanism (Figures 3D,4E). This distinction carries physiological significance: whereas MKRN3 modulates MBD3 under specific developmental or stress contexts [12,18], TRIM59-mediated degradation accounts for the

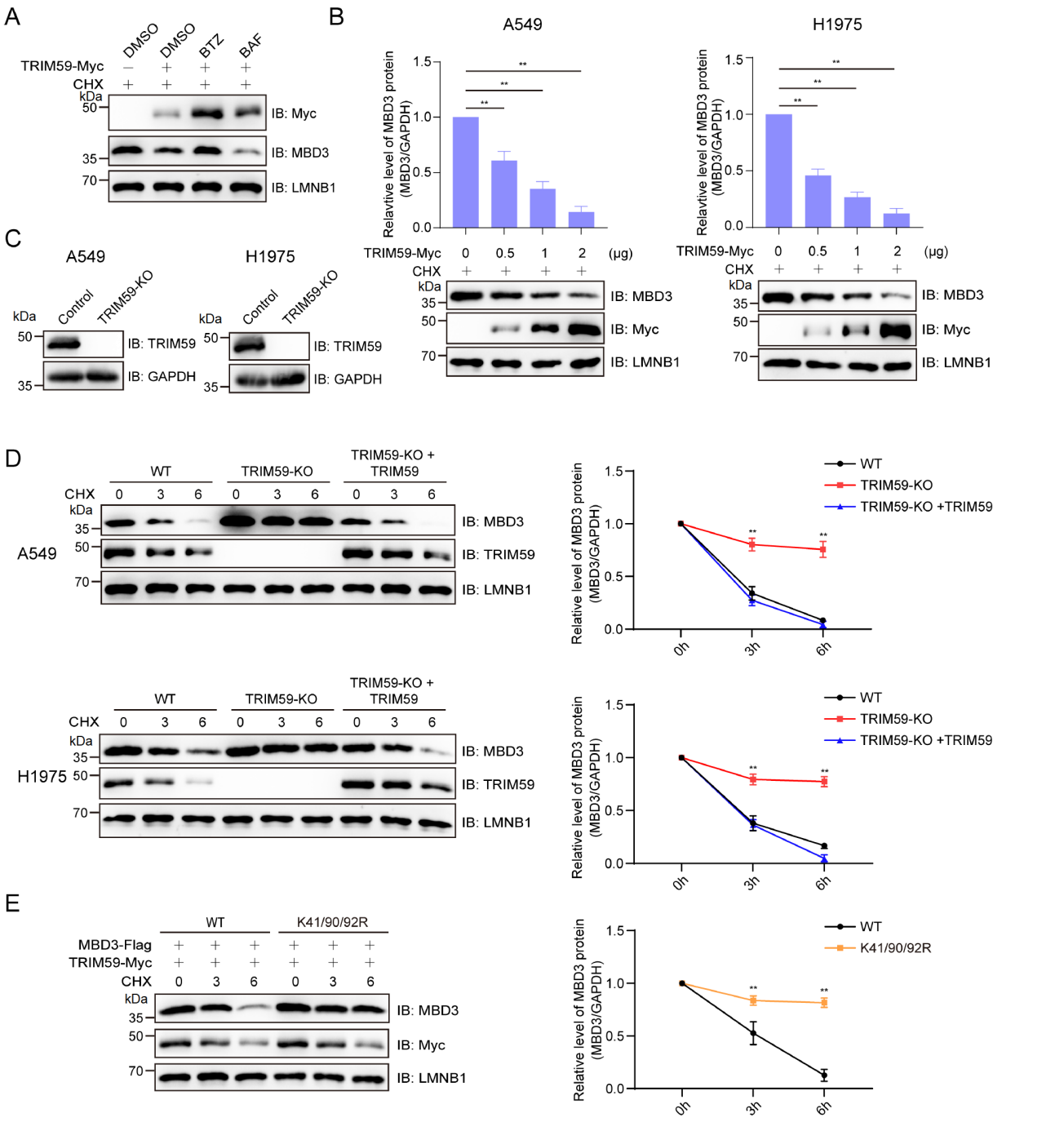


Figure 4. TRIM59 mediates the degradation of MBD3 (A) TRIM59 mediates MBD3 degradation primarily through the proteasomal pathway. A549 cells were treated with CHX for 6 h in the presence or absence of BTZ or BAF prior to harvest. (B) TRIM59 promotes MBD3 degradation in a dose-dependent manner. A549 and H1975 cells were transfected with increasing amounts of TRIM59, treated with CHX for 6 h, and analyzed by immunoblotting. (C) Generation and validation of *TRIM59*-knockout A549 and H1975 cell lines by immunoblotting. (D) *TRIM59* depletion stabilizes MBD3, and this effect is reversed upon reintroduction of TRIM59. A549 and H1975 cells, with or without TRIM59 transfection, were treated with CHX for the indicated durations and then subjected to immunoblot analysis. The experiment was repeated three times and subjected to statistical analysis. (E) TRIM59 destabilizes wild-type MBD3 but not the K41/90/92 mutant. A549 cells were co-transfected with TRIM59-Myc and wild-type or mutant (K41/90/92) MBD3-Flag, treated with CHX for the indicated durations, and analyzed by immunoblotting. The experiment was repeated three times and subjected to statistical analysis. $^{**}P < 0.01$.

systematic destabilization of MBD3 observed in LUAD, thereby explaining the downregulation of this tumor suppressor in malignant tissues.

TRIM59 has emerged as a pleiotropic oncogenic factor across diverse malignancies, including gastric, breast, prostate, and lung cancers [19,20]. As an E3 ubiquitin ligase, TRIM59 regulates the stability of multiple substrates to promote tumorigenesis, including the tumor suppressor p53, the histone variant macroH2A1, and the

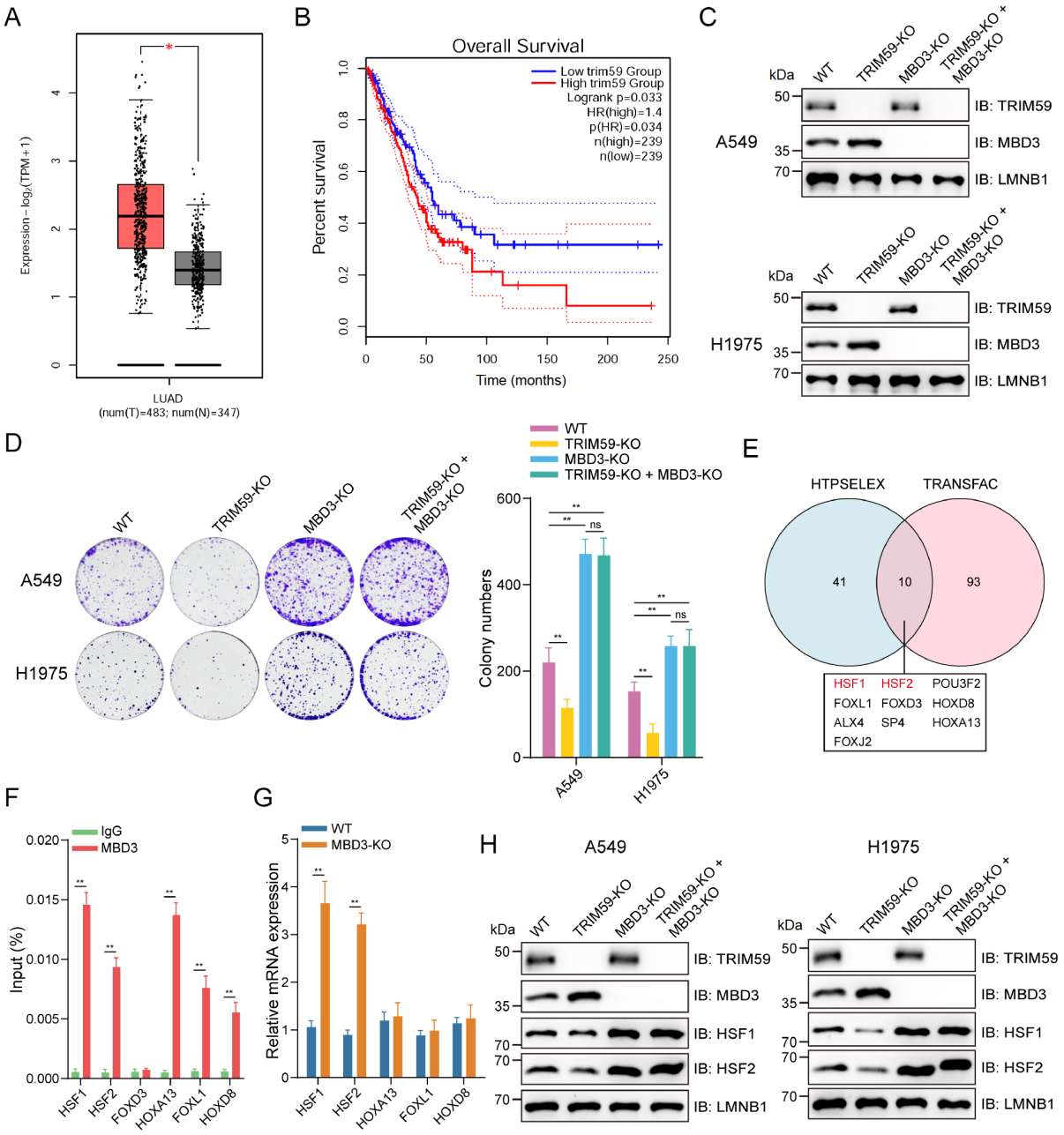


Figure 5. TRIM59 regulates HSF1/2 signaling via MBD3-mediated transcriptional control (A) The mRNA expression levels of *TRIM59* in human LUAD and corresponding normal tissues were analyzed using the GEPIA2 database. (B) Overall survival rates of LUAD patients stratified by TRIM59 expression levels were analyzed using the GEPIA2 database. The solid line represents the survival estimate, and the dashed line represents the 95% confidence interval of the survival curve. (C) Generation and validation of *TRIM59*/*MBD3* double-knockout A549 and H1975 cell lines by immunoblotting. (D) Colony formation assays showed that *TRIM59* depletion inhibits the clonogenic capacity of A549 and H1975 cells. Notably, this inhibitory effect is abrogated in *TRIM59*/*MBD3* double-knockout cells compared to *MBD3* knockout alone. Three replicates per group were performed. (E) Identification of MBD3 target genes through integrative analysis of the HTPSELEX and TRANSFAC databases. High-confidence target sets were intersected and visualized by a Venn diagram. (F) Validation of MBD3 binding to predicted target genes by ChIP in A549 cells. (G) Quantitative PCR analysis of *MBD3*-bound gene expression in wild-type and *MBD3*-knockout A549 cells. (H) *TRIM59* knockdown suppresses HSF1/2 expressions in an MBD3-dependent manner, as concurrent knockout of *MBD3* reverses this inhibition in A549 and H1975 cells. $*P < 0.05$; $**P < 0.01$. ns, no significant difference.

lipolytic factor ABHD5 [21–23]. Additionally, TRIM59 can function as a scaffold protein to stabilize substrates such as PDCD10, preventing their autophagic degradation [24]. The identification of MBD3 extends the TRIM59 oncogenic repertoire to epigenetic regulation. Unlike previous substrates, MBD3 constitutes a NuRD core component whose degradation dismantles epigenetic barriers to derepress protumorigenic genes [11]. This explains how TRIM59 transcends cytoplasmic signaling to reshape chromatin architecture.

HSF1 and HSF2 constitute a critical node in LUAD pathogenesis

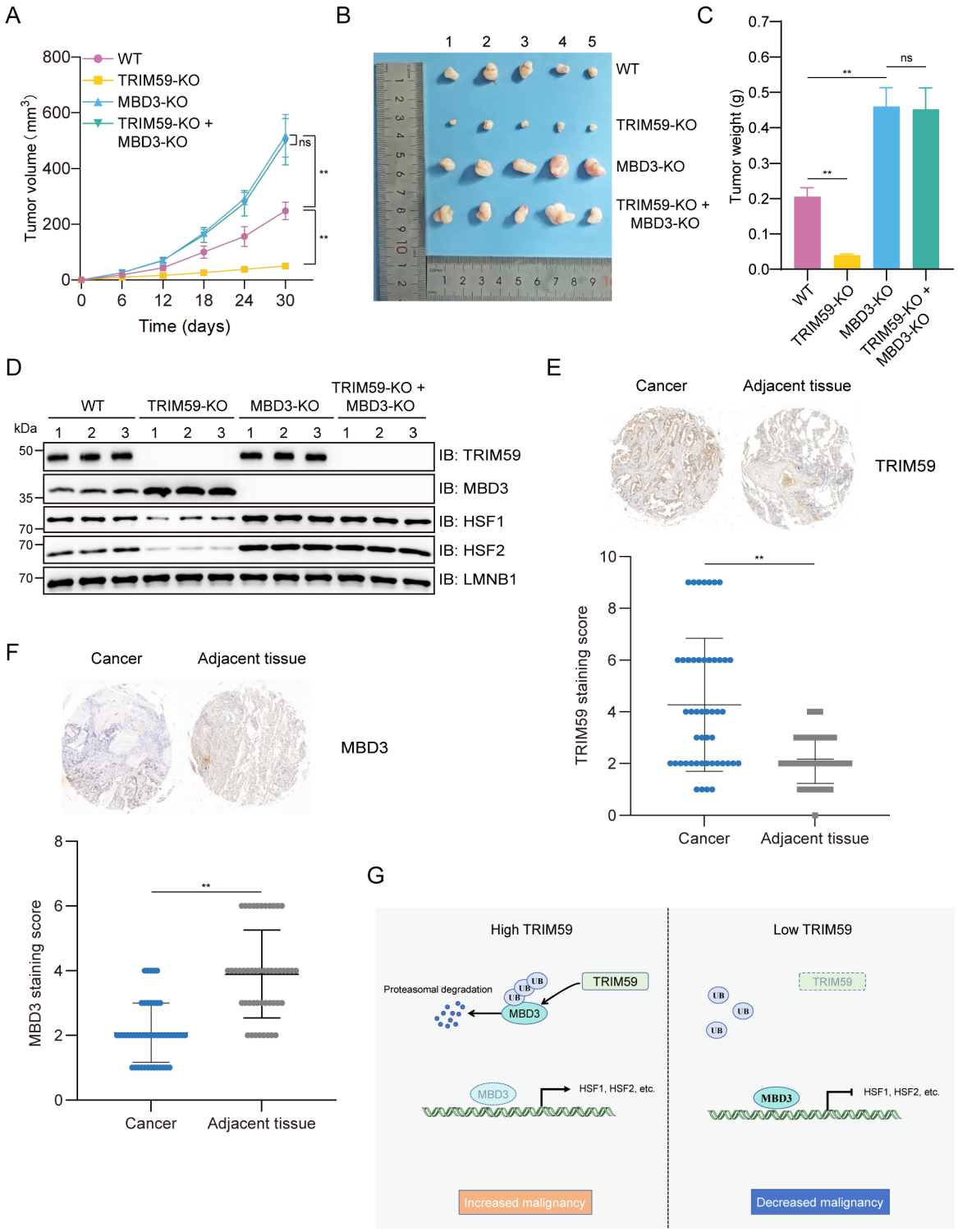


Figure 6. *TRIM59* knockout suppresses LUAD growth via MBD3-dependent HSF1/2 signaling (A) *TRIM59* knockout suppresses tumor growth in nude mice in an MBD3-dependent manner. A549 cells of the indicated genotypes were subcutaneously injected into nude mice, and tumor volumes were measured with digital calipers every 6 days. (B) Representative images of xenograft tumors harvested 30 days after injection of A549 cells of the indicated genotypes. (C) Tumor weights were quantified as the mean ± SD and evaluated by a two-tailed unpaired Student's *t* test. (D) TRIM59, via MBD3, regulates HSF1/2 signaling within xenograft tumors. The protein levels of the indicated proteins were detected by immunoblotting in xenograft tumors from Figure 4B. (E) IHC analysis of tissue microarrays reveals upregulated TRIM59 expression in lung adenocarcinoma. Representative images of cancer and adjacent tissues are shown, and the data were subjected to statistical analysis. (F) IHC analysis of tissue microarrays reveals downregulated MBD3 expression in LUAD. Representative images of cancer and adjacent tissues are shown, and the data were subjected to statistical analysis. (G) A schematic model illustrating how the TRIM59-MBD3 ubiquitin-signaling axis regulates LUAD proliferation. $^{**}P < 0.01$. ns, no significant difference.

[25,26]. HSF1 is well established as a master regulator of the malignant state, driving transcriptional programs that support protein homeostasis, proliferation, and survival under oncogenic stress [27,28]. In lung cancer, HSF1 amplification and nuclear accumulation correlate with advanced disease stage, metastasis, and poor patient prognosis [29]. While HSF2 was traditionally considered dispensable for the heat shock response, recent evidence reveals its cooperation with HSF1 to drive protumorigenic transcriptional programs across breast, prostate, colon, and lung cancers [30,31]. We found that MBD3 binds to the promoters of *HSF1* and *HSF2* to suppress their expression. This positions the TRIM59-MBD3 axis as an upstream regulatory layer that controls the heat shock transcriptional machinery. By degrading MBD3, TRIM59 effectively licenses HSF1/2-mediated transcriptional programs, creating a permissive environment for tumor cell proliferation. This regulatory hierarchy suggests that the oncogenic function of TRIM59 in LUAD is partially mediated through the derepression of heat shock factors, linking the ubiquitin-proteasome system to the stress adaptation mechanisms essential for cancer cell survival.

These findings carry substantial therapeutic implications. The inverse correlation between TRIM59 upregulation and MBD3 downregulation in LUAD suggests that pharmacological inhibition of TRIM59 E3 ligase activity or disruption of the TRIM59-MBD3 interaction could restore MBD3 tumor suppressor function and attenuate HSF1/2-driven malignancy. However, significant challenges remain: the conserved RING domain architecture across the TRIM family complicates the development of specific TRIM59 inhibitors, necessitating future exploration of allosteric inhibitors or TRIM59-targeting PROTACs. While HSF1/2 are critical downstream effectors of MBD3, the potential involvement of additional MBD3-regulated genes cannot be excluded. Furthermore, whether post-translational modifications of TRIM59 itself (*e.g.*, CDK5-mediated phosphorylation reported in other cancers [22]) modulate its activity toward MBD3 in LUAD warrants investigation. Ultimately, clinical translation requires validation through correlative studies linking TRIM59/MBD3/HSF1/2 expression to patient survival and therapeutic responses in large, clinically annotated cohorts, alongside examination of potential crosstalk between TRIM59-MBD3 signaling and established oncogenic drivers such as EGFR and KRAS mutations.

Supplementary Data

Supplementary data are available at *Acta Biochimica et Biophysica Sinica* online.

Data Availability

The mass spectrometry data have been deposited in the OMIX database of the China National Center for Bioinformation/Beijing Institute of Genomics, Chinese Academy of Sciences under accession numbers OMIX015171 and OMIX015173. All other data can be accessed upon reasonable request from the corresponding authors.

Author Contribution

Wenhui Yang: investigation, methodology, designed and performed the main experiments, completed data statistics and drafted the original manuscript; Jin Ren: bioinformatics and mass spectrometry data analysis, and experimental verification; Yufang Wang, Jiahe Shi, Ziwan Cai and Cuihong Cai: reviewed the manuscript; Jing Zheng and Jingjing Qu: funding support; Jianya Zhou: conceptualization, funding support, project management, supervision, writing-review and editing.

Funding

This work was supported by the grants from the Zhejiang Province Pioneer Research and Development Project (Nos. 2023C03069, 2025C02092, and 2025C02094).

Conflict of Interest

The authors declare that they have no conflict of interest.

References

1. Li C, Lei S, Ding L, Xu Y, Wu X, Wang H, Zhang Z, *et al.* Global burden and trends of lung cancer incidence and mortality. *Chin Med J* 2023, 136: 1583–1590
2. Wang Y, Xu M, Wei X, Huang H, Chen Q, Chen B, Bao X, *et al.* Prospective proteomics for discovering biomarkers in lung adenocarcinoma: a literature review. *Transl Cancer Res* 2025, 14: 6102–6117
3. Yu P, Zhang L, Tian J, Liu J, Que Z, Li G, Zhou Y. NK cell depletion promotes liver metastasis of lung cancer cells. *Acta Biochim Biophys Sin* 2024, 56: 323–326
4. Swatek KN, Komander D. Ubiquitin modifications. *Cell Res* 2016, 26: 399–422
5. Sheng X, Xia Z, Yang H, Hu R. The ubiquitin codes in cellular stress responses. *Protein Cell* 2024, 15: 157–190
6. Qiu X, Ren J, Yang Y, Hu W, Wang C, Hu R, Li C. TRIM25 ubiquitinates and degrades p62/SQSTM1 to suppress autophagy. *Acta Biochim Biophys Sin* 2025, 57: 2129–2132
7. Chen T, Xu Y, Yang K, Du Y, Zhu Z, Xu L, Wang X, *et al.* Withaferin A combined with ricolinostat: a potent synergistic therapy for cervical cancer through regulating p53 ubiquitination and acetylation. *Acta Biochim Biophys Sin* 2025, 57: 2133–2136
8. Tao Y, Ding X, Jia C, Wang C, Li C. Using protein turnover assay to explore the drug mechanism of Carfilzomib. *Acta Biochim Biophys Sin* 2024, 57: 209–222
9. Chen J, Yang Y, Liu G, Huang L, Zhang Y, Wang Y, Xu X, *et al.* SUN5 interacts with TRIM28, enhancing IκBα ubiquitination to promote glycolysis in colorectal cancer cells. *Acta Biochim Biophys Sin* 2025, 57: 2094–2109
10. Leighton G, Williams Jr. DC. The methyl-CpG-binding domain 2 and 3 proteins and formation of the nucleosome remodeling and deacetylase complex. *J Mol Biol* 2020, 432: 1624–1639
11. Du Q, Luu PL, Stirzaker C, Clark SJ. Methyl-CpG-binding domain proteins: readers of the epigenome. *Epigenomics* 2015, 7: 1051–1073
12. Li C, Lu W, Yang L, Li Z, Zhou X, Guo R, Wang J, *et al.* MKRN3 regulates the epigenetic switch of mammalian puberty via ubiquitination of MBD3. *Natl Sci Rev* 2020, 7: 671–685
13. Huang K, Zhang B, Feng Y, Ma H. Magnolol promotes the autophagy of esophageal carcinoma cells by upregulating HACE1 gene expression. *Acta Biochim Biophys Sin* 2024, 56: 1044–1054
14. Tang Z, Kang B, Li C, Chen T, Zhang Z. GEPIA2: an enhanced web server for large-scale expression profiling and interactive analysis. *Nucleic Acids Res* 2019, 47: W556–W560
15. Li C, Han T, Li Q, Zhang M, Guo R, Yang Y, Lu W, *et al.* MKRN3-mediated ubiquitination of poly(A)-binding proteins modulates the stability and translation of GNRH1 mRNA in mammalian puberty. *Nucleic Acids Res* 2021, 49: 3796–3813

16. Yang Y, Ren J, Qiu X, Liu Y, Yuan S, Hu R, Xia Z, *et al.* RNF126 writes a non-canonical ubiquitin code on midnolin to tune protein stability. *Acta Biochim Biophys Sin* 2026
17. Xu X, Li C, Gao X, Xia K, Guo H, Li Y, Hao Z, *et al.* Excessive UBE3A dosage impairs retinoic acid signaling and synaptic plasticity in autism spectrum disorders. *Cell Res* 2018, 28: 48–68
18. Palumbo S, Cirillo G, Aiello F, Papparella A, Miraglia del Giudice E, Grandone A. MKRN3 role in regulating pubertal onset: The state of art of functional studies. *Front Endocrinol* 2022, 13: 991322
19. Yamada Y, Kimura N, Maki K, Hakozaki Y, Urabe F, Kimura S, Fujimura T, *et al.* The roles of tripartite motif proteins in urological cancers: a systematic review. *Cancers* 2025, 17: 2367
20. Cen X, Li Z, Chen X. Ubiquitination in the regulation of autophagy. *Acta Biochim Biophys Sin* 2023, 55: 1348–1357
21. Wang Y, Zhou Z, Wang X, Zhang X, Chen Y, Bai J, Di W. TRIM59 is a novel marker of poor prognosis and promotes malignant progression of ovarian cancer by inducing annexin A2 expression. *Int J Biol Sci* 2018, 14: 2073–2082
22. Sang Y, Li Y, Zhang Y, Alvarez AA, Yu B, Zhang W, Hu B, *et al.* CDK5-dependent phosphorylation and nuclear translocation of TRIM59 promotes macroH2A1 ubiquitination and tumorigenicity. *Nat Commun* 2019, 10: 4013
23. Liang M, Chen X, Wang L, Qin L, Wang H, Sun Z, Zhao W, *et al.* Cancer-derived exosomal TRIM59 regulates macrophage NLRP3 inflammasome activation to promote lung cancer progression. *J Exp Clin Cancer Res* 2020, 39: 176
24. Tan P, Ye Y, He L, Xie J, Jing J, Ma G, Pan H, *et al.* TRIM59 promotes breast cancer motility by suppressing p62-selective autophagic degradation of PDCD10. *PLoS Biol* 2018, 16: e3000051
25. Wu L, Feng J, Lin H, Chen P. KNK437 suppresses the growth of non-small cell lung cancer cells by targeting heat shock factor 1. *Drug Dev Res* 2025, 86: e70141
26. Zhong YH, Cheng HZ, Peng H, Tang SC, Wang P. Heat shock factor 2 is associated with the occurrence of lung cancer by enhancing the expression of heat shock proteins. *Oncol Lett* 2016, 12: 5106–5112
27. Zhang B, Fan Y, Tan K. HSF1 activation mechanisms, disease roles, and small molecule therapeutics. *Int J Biol Sci* 2025, 21: 3351–3378
28. Mendillo ML, Santagata S, Koeva M, Bell GW, Hu R, Tamimi RM, Fraenkel E, *et al.* HSF1 drives a transcriptional program distinct from heat shock to support highly malignant human cancers. *Cell* 2012, 150: 549–562
29. Cyran AM, Zhitkovich A. Heat shock proteins and HSF1 in cancer. *Front Oncol* 2022, 12: 860320
30. Himanen SV, Puustinen MC, Da Silva AJ, Vihervaara A, Sistonen L. HSFs drive transcription of distinct genes and enhancers during oxidative stress and heat shock. *Nucleic Acids Res* 2022, 50: 6102–6115
31. Smith RS, Takagishi SR, Amici DR, Metz K, Gayatri S, Alasady MJ, Wu Y, *et al.* HSF2 cooperates with HSF1 to drive a transcriptional program critical for the malignant state. *Sci Adv* 2022, 8: eabj6526